# Estimation of Surface Turbulent Fluxes through Assimilation of Radiometric Surface Temperature Sequences

FRANCESCA CAPARRINI AND FABIO CASTELLI

*Dipartimento di Ingegneria Civile, Università degli Studi di Firenze, Florence, Italy*

DARA ENTEKHABI

*Department of Civil and Environmental Engineering, Massachusetts Institute of Technology, Cambridge, Massachusetts*

(Manuscript received 9 October 2002, in final form 14 July 2003)

ABSTRACT

A model of land surface energy balance is used as a constraint on the estimation of factors characterizing land surface influences on evaporation and turbulent heat transfer from sequences of radiometric surface temperature measurements. The surface moisture control on evaporation is captured by the dimensionless evaporative fraction (ratio of latent heat flux to the sum of the turbulent fluxes), which is nearly constant for near-peak radiation hours on days without precipitation. The dimensionless parameter capturing the turbulent transfer characteristics (bulk heat transfer coefficient) includes the impacts of both forced and free convection. The mean diurnal pattern and seasonal trends are interpreted in the context of expected surface air layer static stability variations.

The approach is tested over the First International Satellite Land Surface Climatology Project (ISLSCP) Field Experiment (FIFE) site (Kansas) where verification data on surface fluxes are available. It is shown that sequential radiometric surface temperature data contain useful information on the partitioning of available surface energy and may even be used to infer some key characteristics of surface turbulent transfer. The land data assimilation scheme is formulated such that it does not require auxiliary data on soil texture and vegetation. Feasibility of extending the land data assimilation to use remote sensing measurements is tested by simulating the observing system sampling based on field experiment measurements. Applications with remote sensing data would allow large-scale mapping of land surface energy balance components.

## 1. Introduction

The estimation of surface energy balance and the exchange of mass and energy from land to atmosphere is required in many applications in hydrology, meteorology, and ecology. The partitioning of available energy into turbulent fluxes of heat and moisture is dependent on the moisture status of the soil–vegetation continuum. The magnitude of the combined turbulent fluxes and their relative partitioning affect the development of the boundary layer and act to force the dynamics of the lower troposphere.

There are no ground-based networks of surface flux and energy balance measurements that can provide mapping of these variables. In situ measurements of turbulent fluxes and surface moisture influence on the partitioning among energy balance components are difficult and costly. There are measurements available from a handful of sparse flux tower networks (e.g., Fluxnet and Ameriflux) and a few limited-area and short-duration field experiments [e.g., First International Satellite Land Surface Climatology Project (ISLSCP) Field Experiment (FIFE), Boreal Ecosystem–Atmosphere Study (BOREAS)] but the use of point values to infer regional conditions (mapping) are hampered by the presence of strong spatial heterogeneity in factors such as surface moisture, vegetation cover, and terrain.

The key problem is how to use now-available spaceborne observations to make quantitative inferences about surface energy balance components, especially the magnitude and partitioning among surface turbulent fluxes (sensible $H$ and latent LE). If the relations between remote sensing measurements and these fluxes are confirmed, mapping of the energy balance components will be a major new capability for understanding and predicting variations in global and regional water, energy, and biogeochemical cycles.

For the problem of estimating energy balance components and especially the latent and sensible heat fluxes, the two most challenging effects to capture are: 1) surface boundary influence on near-surface turbulence, and 2) surface controls on the partitioning among sen-

*Corresponding author address:* Dara Entekhabi, Department of Civil and Environmental Engineering, Massachusetts Institute of Technology, Cambridge, MA 02139.
E-mail: darae@mit.edu

sible and latent heat fluxes. The first effect is often represented by bulk transfer coefficients ($C_D$ drag coefficient for momentum and $C_H$ for heat) or by roughness length scales (scalar roughness $z_{0M}$ for momentum transfer and $z_{0H}$ for heat). Bulk transfer coefficients, when multiplied by wind speed at a reference elevation, become the proportionality parameter equating turbulent flux and differences in surface and near-surface properties. For the second effect (surface control on $H$ and LE partitioning) the Bowen ratio ($H$/LE), or evaporative fraction [LE/(LE + $H$)], may be used to capture the dynamics. Surface control here refers to the reduction of evaporation below its energy-limited value through resistances imposed by plant physiology or soil pore tension. The question is how to relate standard in situ or remote sensing measurements, in the absence of a direct or unique relationships, to these critical parameters. For the roughness length scales parameter, there are attempts that rely on empirical relations to canopy geometry. These approaches then use remote sensing of canopy properties to map fields of the parameter (e.g., Jasinski and Crago 1999; Schaudt and Dickinson 2000). For the surface control on turbulent flux partitioning, the focus has been on direct (using low-frequency microwave; e.g., Cahill et al. 1999) and indirect (using visible and thermal imaging) methods to estimate soil moisture.

There is extensive history of using thermal remote sensing and land surface temperature for the estimation of land evaporation. One approach is to estimate surface soil moisture, which can then be used to infer evaporation using models. The diurnal amplitude of the land surface temperature depends on the thermal inertia of the medium. The thermal inertia of soils is significantly affected by the water content and it can be shown to be proportional to the diurnal amplitude of the ground heat flux divided by the diurnal amplitude of the land surface temperature, that is, $P \sim \Delta G/\Delta T$. The latter can be measured using satellite observations (e.g., Carlson 1986; Carlson et al. 1981; Jackson 1982; Price 1982). The ground heat flux amplitude has to be empirically related to other factors such as net radiation or land cover type (Idso et al. 1976). Alternatively it can be found by driving a model of surface energy budget using micrometeorology. Nevertheless reconciling the satellite estimates of diurnal land surface temperature amplitude and the one implicitly required to estimate the ground heat flux amplitude remains an unsolved problem. Furthermore the inference of evaporation from thermal inertia-based soil moisture requires further modeling and parameterization.

Another historical framework for the use of remotely sensed land surface temperature in surface flux estimation is to use the apparent correlations between evaporation, temperature, and vegetation state. Scatterplots of vegetation index (VI) and land surface temperature show that regions with similar soil moisture or evaporation tend to group together (Nemani and Running 1989). There have been various extensions of this method using different normalization procedures. Furthermore methods have been developed for using VI and land surface temperature in the inversion of soil–vegetation–atmosphere transfer schemes and estimation of fluxes (Carlson et al. 1995a; Gillies et al. 1997). The so-called triangle method has been extended and applied in a number of studies (e.g., Moran et al. 1994; Jiang and Islam 2001).

There are also many studies in the literature that use statistical relationships (e.g., regression) relating the surface energy balance components and VI (Carlson et al. 1995b). Beyond the empirical approaches there have been many studies that estimate the components of the energy balance through the land surface temperature state $T_s$. Because the surface energy balance depends not only on the surface temperature state but also on its time tendency $dT_s/dt$, often closure assumptions need to be invoked. Otherwise the system is not uniquely invertible. Moreover any noise in the surface temperature measurements overwhelms the true value of the tendency term in the energy balance. The most common closure is to empirically relate the amplitude of the ground heat flux to the noontime net radiation at the soil surface as in $G = cR_{n,\text{soil}}$ (Mecikalski et al. 1999; Norman et al. 2000). The proportionality $c$ coefficient is taken to be 10%–30% or related to VI, and surface temperature differences between early and late morning are used to reduce the noise in the sensible heat estimation.

More recently Xu and Qiu (1997), Zhou and Xu (1999), and Ma and Daggupaty (2000) take the further step of estimating surface roughness length parameters in addition to sensible and latent heat fluxes. Their retrieval approach requires two-level surface air micrometeorology that are generally not available at standard stations and cannot be inferred from remote sensing data.

This study introduces a new approach to using land surface temperature to estimate surface fluxes. In a departure with previous approaches, neither of the previously mentioned assumptions (estimation of thermal inertia $P \sim \Delta G/\Delta T$, empirical relation $G = cR_{n,\text{soil}}$, statistical VI–temperature–flux relations as in triangle method) are used. Instead the new approach uses the implicit information that is contained in *sequences* of radiometric surface temperature measurements to estimate both surface boundary effects on turbulence as well as moisture-related surface control on the partitioning among turbulent fluxes. The estimation is feasible because it merges noisy land temperature measurements and surface energy balance physical constraint in a variational data assimilation scheme. The scheme has long been used in data assimilation with significant history of geophysical applications (Sun 1994). The objective of this study is to develop a methodology that can then be scaled to use in conjunction

with remote sensing data that enable mapping of the energy balance components.

This study builds on Castelli et al. (1999) and Boni et al. (2000) that show the data assimilation methodology (adjoint-state variational scheme) to be effective in inferring information about surface moisture control on evaporation from sequences of land surface temperature measurements. In these earlier studies the objective of the estimation was specific humidity at the surface. Together with land surface temperature and micrometeorological measurements, surface fluxes can be calculated from specific humidity at the surface. In this new study the problem has matured to focus on the estimation of the two challenging and more fundamental parameters in land influence on surface fluxes (as discussed earlier: EF and a measure of the bulk turbulent transfer coefficient). The problem is similarly formulated in the adjoint-state variational framework. Land surface temperature sequences are again used.

Land surface temperature can be estimated with reasonable accuracy (with reference to the magnitude of perturbations in the variable) from satellites operating in the thermal infrared (Pozo Vazquez et al. 1997; Qin and Karnieli 1999) under clear sky conditions. Passive microwave sensors can also be used for land surface temperature retrieval under cloud cover (McFarland et al. 1990; Prigent and Rossow 1999; Williams et al. 2000). Several space platforms carry instruments that can be used to infer land surface temperature.

In this study we introduce the methodology to use such measurements to derive estimates of the surface components of the energy balance. We test the approach using field experiment data. In observing system simulation tests we evaluate the sources and magnitudes of temporal sampling errors introduced in using spaceborne measurements.

## 2. Estimation objectives

### a. Surface effects on turbulent transfer

The parameters estimated in the land assimilation system of this study are surface moisture control on evaporation and characteristics of turbulent transfer, that are both required in order to retrieve surface fluxes. Using a bulk transfer formulation, sensible and latent heat fluxes can be expressed in terms of the gradients of air temperature ($T$) and humidity ($q$) from the land surface (subscript $s$) to the atmosphere (subscript air):

$$H = \rho c_p C_H U(T_s - T_{\text{air}}) \tag{1}$$

$$\text{LE} = \rho L C_E U(q_s - q_{\text{air}}), \tag{2}$$

where $U$ is wind speed and $c_p$ and $L$ are thermodynamic properties (air specific heat and latent heat of vaporization). The dimensionless parameters $C_H$ and $C_E$ are bulk transfer coefficients for heat and moisture. In this application we assume a common bulk scalar turbulent transfer coefficient $C_B$ for heat and humidity.

Buoyancy effects on $C_B$ can be accounted for using empirical functions that depend on the ratio between buoyancy and wind shear in generating turbulence. We expect $C_B$ to increase during the daytime, when the atmosphere tends to be unstable and there is more turbulence, and then decrease again in the afternoon. The dimensionless quantity that characterizes the degree of atmospheric stability is the Richardson number (flux, gradient and bulk). Bulk Richardson number is negative under unstable conditions and it can be calculated as a diagnostic from micrometeorological measurements:

$$\text{Ric}_B = \frac{g}{\theta}\frac{\Delta\theta\Delta z}{(\Delta U^2)}, \tag{3}$$

where $g$ is gravitational acceleration, $\Delta\theta$ is potential temperature gradient across height difference $\Delta z$, and $U$ is wind speed.

### b. Surface moisture–related effects on partitioning of turbulent fluxes

The other governing factor in the determination of surface fluxes is related to surface control on latent heat flux. Usually, surface control on evaporation is formulated either expressing the real evaporation $E$ as a fraction of the energy-limited (potential evaporation $E_{\text{pot}}$ for a adequately moist surface), or expressing the specific humidity at the ground surface, $q_s$, by reducing the temperature-dependent saturation specific humidity. Mahfouf and Noilhan (1991) present an overview of the different approaches. In this study the objective is to directly estimate the evaporative fraction, EF given as

$$\text{EF} = \frac{\text{LE}}{\text{LE} + H}, \tag{4}$$

which is normally a diagnostic of surface energy balance. Once EF is known, then (1) and (2) can be written as

$$\text{LE} = \frac{\text{EF}}{1 - \text{EF}}H. \tag{5}$$

Given temperature estimates, the evaporation rate can then be estimated.

It has been demonstrated that the evaporative fraction is approximately constant for near-peak radiation hours on days without precipitation (Crago 1996; Crago and Brutsaert 1996). Therefore this parameter is a suitable candidate for a robust retrieval in the data assimilation scheme.

### c. Constraints on estimation

Estimation of $C_B$ and EF from sequences of land surface temperature is made by imposing a physical constraint. The constraint is given by a system equation that governs the evolution of the land surface temperature-state variable. Here the system equation is the *force–restore* approximation to the surface temperature of a

medium with constant effective thermal inertia $P_e$ (Bhumralkar 1975). The model gives time evolution of land surface temperature $T_s$ in response to atmospheric forcing ($R_n - H - \mathrm{LE}$) with a dominant (diurnal) frequency $\omega$ and to the restoring effect of a restoring temperature $T_D$ as

$$\frac{dT_s}{dt} = \left(\frac{2\sqrt{\pi\omega}}{P_e}\right)(R_n - H - \mathrm{LE}) - 2\pi\omega(T_s - T_D). \quad (6)$$

Here $R_n$ is the net radiation at the surface of the medium. This simple thermal balance model captures the apparent dynamic of land surface temperature—as remotely sensed—which is the result of complicated (possibly intractable) heat transfer processes within the canopy and the soil subsurface. The heat fluxes ($H$, LE, and $R_n$) depend on the land surface temperature state. There is however a distinction between radiometric land surface temperature (observed using radiometers and used in $R_n$) and aerodynamic land surface temperature (used in $H$ and LE). When radiometric land temperature is used to estimate the turbulent fluxes, then the turbulent transfer coefficient takes on a different definition. For example, Sugita and Brutsaert (1990) estimate surface turbulent fluxes using radiometric skin temperature for the land surface temperature. In that case the estimated scalar roughness for heat transfer is called the radiative scalar roughness.

In this assimilation study the retrieved values of $C_B$ represent land surface energy balance modeling with radiometric surface temperature. The retrieved values of $C_B$ are therefore consistent with using radiometric land surface temperature in turbulent flux calculations. This approach is in preparation for using the large volumes of available satellite remote sensing data to map energy balance components over land regions.

Radiometric land surface temperature (here, the state variable $T_s$) has emission contributions from the soil surface and the temperature profile within the vegetation canopy. The difference between the sensed radiometric temperature and an equivalent isothermal temperature for the vegetated land surface is generally small (order of 1 K) unless the surface is viewed from very near nadir, the temperature gradient within the canopy is large, and the canopy is sparse (Matsushima and Kondo 1997; Crago 1998). The dynamics of the thermal model (6) for $T_s$ in response to atmospheric forcing is controlled by two factors: the effective thermal inertia $P_e$ of the medium and the restoring temperature $T_D$.

The soil and the canopy media have disparate thermal properties that factor in the effective properties for the model in (6). Dickinson (1988) gives generalizations of the force–restore thermal model for conditions when the forcing has significant variability in several frequencies and for conditions where there is layered media with different thermal properties. The critical factor that weights the thermal properties of a two-layer model into the effective thermal properties is $\exp(-2h/l)$ where $h$ is the depth of the top medium (vegetation canopy) and $l$ is the penetration $e$-folding depth of the principal heat wave (Dickinson 1988). The upper medium properties and lower stratum properties are weighted by $1 - \exp(-2h/l)$ and $\exp(-2h/l)$, respectively. The penetration depth length scale is related to the top media thermal conductivity $\lambda$ and volumetric heat capacity $c$ as in $l = \sqrt{2\lambda/c\omega}$. The value for heat capacity $c$ for a canopy layer may be reasonably estimated from the mixing ratios of the layer constituents, the value for the thermal conductivity $\lambda$ depends mostly on the height of the canopy and turbulence decay down the layer. A conservative value, for example, a lower limit, of about 3 m for the penetration depth $l$ may be estimated assuming that the canopy-layer heat capacity is about the double of dry air and the average turbulent conductivity within the canopy is about one order of magnitude smaller than the earlier canopy air layer (Raupach 1989). The weighting $\exp(-2h/l)$ of the thermal conductivity and the penetration depth result in an effective thermal inertia that is below that of soil but of the same order of magnitude for a tall grass prairie—here taken to be $\sim$750 J m$^{-2}$ K$^{-1}$ s$^{-1/2}$. Examples of typical values of thermal inertia are (Stull 1994) $\sim$1500 J m$^{-2}$ K$^{-1}$ s$^{-1/2}$ for sandy clay soil with 15% moisture content and $\sim$600 J m$^{-2}$ K$^{-1}$ s$^{-1/2}$ for dry quartz sand.

A consistent value for the restoring temperature $T_D$ is estimated by matching the phase-lagged and filtered land surface temperature $T_s$ with the analytic solution of the heat diffusion equation. The restoring temperature for the diurnal temperature wave is thus found by applying a semidiurnal filter to land surface temperature with diurnal frequency $\omega$ and amplitude $A$:

$$T_D = \frac{2A}{\Delta t}\int_{t-\Delta t/4}^{t+\Delta t/4} \sin[\omega(\tau - \tau^*)]\, d\tau$$

$$= \frac{2}{\pi}A \sin[\omega(t - \tau^*)]. \quad (7)$$

The analytic solution has damped amplitude $Ae^{-z/l}$ and phase-lag $-z/l$ for the temperature fluctuations away from the $z = 0$ where the Dirichlet boundary condition $T(z = 0, t) = \mathrm{A} \sin[\omega t]$ is applied. The required phase-lag may now be found by matching the amplitudes and phases ($2/\pi = e^{-z/l}$ and $\omega\tau^* = z/l$) that yields $\tau^* = \Delta t/2\pi \ln(\pi/2)$ or phase-lag of $\sim$2 h for the semidiurnal filter.

## 3. The variational scheme

The data assimilation problem is formulated in an adjoint-state variational scheme (Sun 1994). This scheme allows the estimation of an unknown parameter vector $\mathbf{Y}$ given measurements of a state vector $\mathbf{X}$ in the case where they are related through the initial value problem in $t \in (t_0, t_1)$:

$$\frac{d\mathbf{X}}{dt} = F(\mathbf{X}, \mathbf{Y}) \tag{8}$$

$$\mathbf{X}(t_0) = \mathbf{X}_0. \tag{9}$$

An important advantage of variational techniques is that they are batch estimators in that they use all the measurements in the assimilation period $(t_0, t_1)$ to estimate the parameters $\mathbf{Y}$. In this respect, they are often superior to sequential approaches such as the recursive Kalman filter where only the measurements up to the update time are used. The assimilation is based on the minimization of a penalty function $J$, which incorporates the squared errors on state predictions with respect to available measurements $\mathbf{X}'$ and parameters estimation with respect to ''prior'' values $\mathbf{Y}'$. The physical constraint given by the earlier initial value problem is adjoined through Lagrange multipliers $\boldsymbol{\lambda}$:

$$J(\mathbf{X}, \mathbf{Y}) = \int_{t_0}^{t_1} (\mathbf{X} - \mathbf{X}')^{\mathrm{T}}\mathbf{K}_X(\mathbf{X} - \mathbf{X}')\, dt + J_Y[(\mathbf{Y} - \mathbf{Y}')^{\mathrm{T}}\mathbf{K}_Y(\mathbf{Y} - \mathbf{Y}')] + \int_{t_0}^{t_1} \boldsymbol{\lambda}^{\mathrm{T}}\left[\frac{d\mathbf{X}}{dt} - F(\mathbf{X}, \mathbf{Y})\right] dt. \tag{10}$$

The function $J_Y$ represents a general quadratic measure of the quantity $(\mathbf{Y} - \mathbf{Y}')$. In defining the earlier penalty function we implicitly assume that the initial condition $\mathbf{X}_0$ is known independently of the estimated values for the parameters $\mathbf{Y}$. We can assume different functional forms for $J_Y$ depending on whether the parameters $\mathbf{Y}$ are time-variant or constant. The values $\mathbf{K}_X$ and $\mathbf{K}_Y$ are matrices of numerically constant parameters whose relative magnitude controls the rate of convergence of the iterative minimization procedure described later. Their absolute magnitude may be also related to the inverse covariance functions of measurement and parameter estimation errors (Bennett 1992). The best estimate, in a least squares sense, of the parameters $\mathbf{Y}$ is found by minimizing the function $J$ so that the forecast error and physical constraint mismatch terms are all minimized. This is accomplished by equating the first variation of $J$ with respect to $\mathbf{X}$ and $\mathbf{Y}$ to zero:

$$\delta J = \int_{t_0}^{t_1} [(\mathbf{X} - \mathbf{X}')^{\mathrm{T}}\mathbf{K}_X\delta\mathbf{X} + \delta\mathbf{X}^{\mathrm{T}}\mathbf{K}_X(\mathbf{X} - \mathbf{X}')]\, dt + \frac{\partial J_Y}{\partial \mathbf{Y}}\delta\mathbf{Y} + \int_{t_0}^{t_1} \boldsymbol{\lambda}^{\mathrm{T}}\left(\frac{d\delta\mathbf{X}}{dt} - \frac{\partial F}{\partial \mathbf{X}}\delta\mathbf{X} - \frac{\partial F}{\partial \mathbf{Y}}\delta\mathbf{Y}\right) dt = 0. \tag{11}$$

The time derivative in the Lagrangian term can be integrated by parts, so that the various terms may be grouped according to independent variations $\delta\mathbf{X}$ and $\delta\mathbf{Y}$. The Euler–Lagrange equations can then be finally obtained as

$$\frac{d\boldsymbol{\lambda}}{dt} = -\boldsymbol{\lambda}^{\mathrm{T}}\frac{\partial F}{\partial \mathbf{X}} + (\mathbf{X} - \mathbf{X}')^{\mathrm{T}}\mathbf{K}_X \tag{12}$$

$$\boldsymbol{\lambda}(t_1) = (\mathbf{X} - \mathbf{X}')^{\mathrm{T}}\mathbf{K}_X|_{t=t_1} \tag{13}$$

$$\frac{\partial J_Y[(\mathbf{Y} - \mathbf{Y}')^{\mathrm{T}}\mathbf{K}_Y(\mathbf{Y} - \mathbf{Y}')]}{\partial \mathbf{Y}} = \int_{t_0}^{t_1} \boldsymbol{\lambda}^{\mathrm{T}}\frac{\partial F}{\partial \mathbf{X}}\, dt. \tag{14}$$

Note that the differential problem for the Lagrange multipliers $\boldsymbol{\lambda}$ is forced by the misfit between state predictions and measurements. The optimal solution to the assimilation problem is reached through an iterative procedure, which includes the following fundamental steps:

1) Integrate the system equation (8) with the prior estimate of the parameters $\mathbf{Y}'$ and current prediction of the state $\mathbf{X}$;
2) integrate the Euler–Lagrange equation (12) using current estimation of the Lagrange multiplier vector $\boldsymbol{\lambda}$;
3) update parameters vector $\mathbf{Y}$ from its prior $\mathbf{Y}'$ with a correction proportional to $\boldsymbol{\lambda}$ as in (14).

The iterative procedure tends to converge—for well-posed problems—to vanishing values of $(\mathbf{X} - \mathbf{X}')$ and hence $\boldsymbol{\lambda}$. In practice, model and measurements errors need to be taken into account, so that the iterative procedure is stopped when some finite converge criterion is achieved. A convenient choice, also adopted in this application, is to stop the iterations when either the magnitude of the mismatch term $(\mathbf{X} - \mathbf{X}')$ goes below the mean-square error of the available measurements $\mathbf{X}'$ or a predefined maximum number of iterations is reached.

In this assimilation study, we have $\mathbf{X} = T_s$, that is, a single-component vector, while $\mathbf{Y} = [C_B, \mathrm{EF}]$, that is, a two-component vector. Here, $C_B$ and EF are also assumed to be statistically independent, so that $\mathbf{K}_Y = \mathrm{diag}\,[K_{C_B}, K_{\mathrm{EF}}]$. Using (6) as the model constraint, the set of Euler–Lagrange equations is now

$$\frac{d\lambda}{dt} = \lambda\left(2\pi\omega + \frac{\partial\Gamma}{\partial T_s}\right) + K_{T_s}(T_s - T_{s,\mathrm{obs}}) \tag{15}$$

$$\lambda(t_1) = K_{T_s}(T_{s,\mathrm{obs}} - T_s)|_{t=t_1} \tag{16}$$

$$\frac{\partial J_{C_B}}{\partial C_B} = -\frac{1}{K_{C_B}}\int_{t_0}^{t_1} \lambda\frac{\partial\Gamma}{\partial C_B}\, dt \tag{17}$$

$$\frac{\partial J_{\mathrm{EF}}}{\partial \mathrm{EF}} = -\frac{1}{K_{\mathrm{EF}}}\int_{t_0}^{t_1} \lambda\frac{\partial\Gamma}{\partial \mathrm{EF}}\, dt, \tag{18}$$

where, after having inverted (4) for $\mathrm{LE} = H \cdot \mathrm{EF}/(1 - \mathrm{EF})$ and substituted (1) into (6), it is

$$\Gamma(T_s, C_B, \mathrm{EF}) = \frac{2\sqrt{\pi\omega}}{P_e}\rho c_p C_B U\frac{(T_s - T_{\mathrm{air}})}{1 - \mathrm{EF}}. \tag{19}$$

Since $\partial J_{C_B}/\partial C_B = f(C_B - C_B')$ and $\partial J_{\mathrm{EF}}/\partial \mathrm{EF} = f(\mathrm{EF} - \mathrm{EF}')$, (17) and (18) are update equations for the parameters $C_B$ and EF. The forms of $J_{C_B}$ and $J_{\mathrm{EF}}$ are different depending on time resolution of update and var-

TABLE 1. Measurements of micrometeorological variables and surface properties required (in addition to land surface temperature) in the assimilation scheme depending on different radiation measurements availability. If net radiation measurements are available (configuration A), only air temperature and wind speed are necessary. In other cases (configurations B to D), additional measurements are required for the computation of radiation budget components: surface albedo for reflected solar radiation and air humidity for the estimation of incoming terrestrial radiation.

| | Micrometeorological measurements and surface properties required in the assimilation scheme | | | | | | | |
|---|---|---|---|---|---|---|---|---|
| | Air temperature | Wind speed | Air humidity and pressure | Net radiation | Incoming SW radiation | Net SW radiation | Incoming SW and incoming LW | Albedo |
| Configuration A | X | X | | X | | | | |
| Configuration B | X | X | X | | X | | | X |
| Configuration C | X | X | X | | | X | | |
| Configuration D | X | X | | | | | X | X |

iability of parameters to be estimated. They are specified in the various cases in the forthcoming sections.

The inverse problem, outlined in this general form, may be ill posed. If both EF and $C_B$ are allowed to vary in time at the same resolution of observed states, they cannot be simultaneously estimated on the basis of a single adjoint model equation. This crucial point will be solved in the applications described next by adding further constraints on the time variability and ranges for the estimated parameters.

## 4. Model tests at FIFE

The model is tested using forcing and independent validation data from the First ISLSCP Field Experiment that took place in Kansas, during the summer of 1987 and 1988 (Sellers et al. 1992). The longest contiguous days of the FIFE experiment (from Julian days 148 to 242 in 1987 and 160 to 242 in 1988) are used for the data assimilation application and validation. The predominant land cover of the experimental site is grass prairie. Measurements of micrometeorological variables and surface fluxes (which we use for independent validation) were averaged and reported every 30 min (48 observations per day). The Betts and Ball (1998) dataset used here is area-averaged based on several stations over the 15 km by 15 km study area. During the summers of 1987 and 1988 the number of deployed instruments and measurement stations (including their location) changed considerably. The Betts and Ball (1998) dataset applies quality-control and weighted-averaging procedures to produce the area-effective data (see citation for full detail).

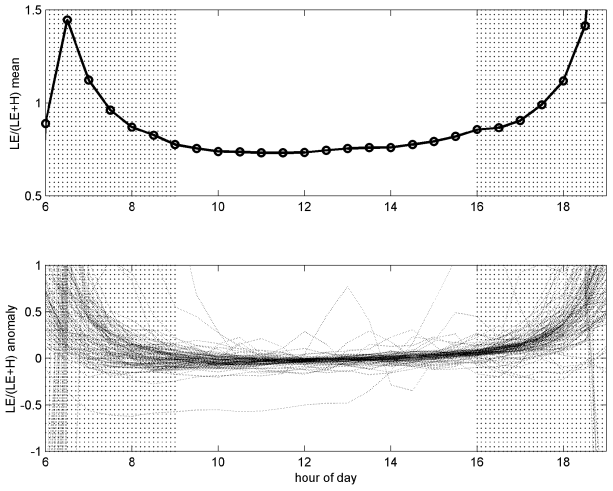


FIG. 1. (top) Mean diurnal cycle of mesured evaporative fraction [EF = LE/(LE + $H$)] for FIFE 1987 (from Julian day 148 to 242). (bottom) Half-hour EF anomaly with respect to the diurnal average (0900–1600 LT) of each day. Both plots are shadowed outside the assimilation window (0900–1600 LT).

The required micrometeorological forcing data are net radiation, air temperature, and wind speed. Neither precipitation nor humidity measurements are used in the assimilation. Other measurements like air humidity and pressure may be necessary if (a) relevant air density variations are to be taken into account, or (b) longwave radiation emitted from the atmosphere is not directly measured and has to be computed (see Table 1 for different data configurations, which mostly differ in terms of data required to estimate the radiation budget components). In this study, air density variations are considered as a second-order correction and are not taken into account and net radiation measurements were available, so that neither air humidity nor pressure measurements have been used. No information on landscape (land use classification, soil properties, etc.) are provided to the assimilation system.

In this first test of the assimilation procedure all the radiometric data (half-hourly) are used, but in further applications undersampled measurements that anticipate application with low-earth-orbit satellite measurements are used instead. The assimilation scheme is applied to daytime fluxes [between 0900 and 1600 local time (LT)] when the hypothesis of constant EF holds. To verify this hypothesis, Fig. 1 shows the average ratio of FIFE field-measured LE over the sum of measured LE and $H$ for the period of the experiment in 1987. The evaporative fraction EF is nearly constant during near-peak radiation hours and over the assimilation window. Day-to-day variations of EF reflect wetting and drydown events.

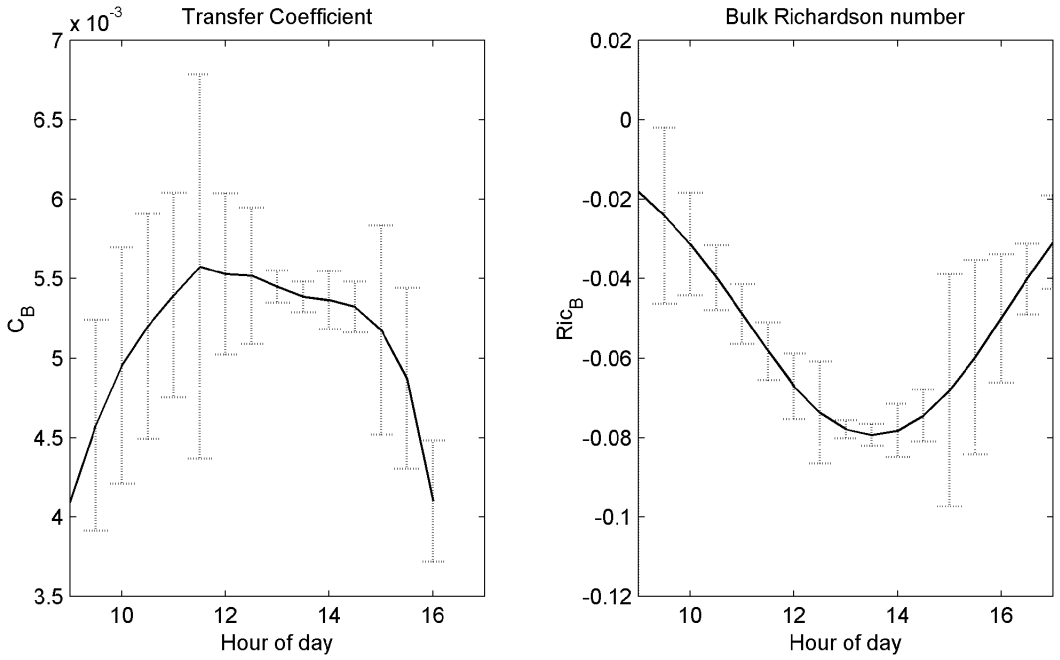


FIG. 2. Mean diurnal cycle of the retrieved transfer coefficient and bulk Richardson number (results for FIFE 1987). Standard error bars ($\pm\sigma$) are also represented.

*a. First experiment: Assimilation with known evaporative fraction*

The estimation problem is approached incrementally in order to better understand the degree to which the system is well or ill posed, as anticipated at the end of section 3. The first experiment is focused on the assimilation of a single parameter $R$ that is related to the neutral component of the bulk heat transfer coefficient with radiometric temperature as in $(C_B)_N = e^R$. The transformation is introduced in order to ensure $C_B > 0$. Evaporative fraction values are set to their known daily EF estimated from FIFE field measurements of latent and sensible heat fluxes. The retrieved transfer coefficient (estimated half-hourly) captures both the surface roughness and the atmospheric stability effects in inducing turbulence. In this case we can set $J_{C_B} = J_{C_B}(R) = \int_{\tau_0}^{\tau_1} (R - R')^2 \, d\tau$ and the update equation (17) for the parameter $R$ becomes

$$R = R' - \frac{1}{K_{C_B}} \lambda \frac{\partial \Gamma}{\partial R}. \tag{20}$$

Figure 2 shows the diurnal cycle of the retrieval $C_B$. The pattern is consistent with stability conditions of the atmosphere during the day. This effect is shown by also plotting the bulk Richardson number diurnal cycle at the same site. Both parameters exhibit diurnal variations with a peak around midday, when there is greater turbulence generation by free convection. Day-to-day variability is captured by the error bars around the mean estimate. Using different surface-layer parameterization methods, Chen et al. (1997) computed instantaneous values of $C_B$ at the FIFE site ranging from about 0.001 to 0.035 and 0.04 for 2 weeks of, respectively, June and August 1987.

The relation between nonneutral transfer coefficient and stability indicators such as Richardson number or Monin–Obukhov length presented in the literature are empirical and do not apply to the generality of cases. Moreover, such functions usually require either iterative procedures to solve for friction velocity $u_*$ and temperature scale $\theta_*$ or a priori assumptions on surface characteristics such as roughness length (Van den Hurk and Holstslag 1997). In this study the experimental results are used to construct a simple stability-correction function of the form

$$\frac{C_B}{(C_B)_N} = f(\mathrm{Ric}_B) = 1 + e^{\Psi}(1 - e^{10\,\mathrm{Ric}_B}). \tag{21}$$

Other functional forms and dependencies for the stability correction may be used. The value of $(C_B)_N$ is deduced by analyzing the retrieved $C_B$ for $\mathrm{Ric}_B \to 0$. Figure 3 shows the 0900–1600 LT average values of the retrieved $C_B/(C_B)_N$ versus averages of $(-\mathrm{Ric}_B)$. Different symbols indicate different periods of the experiment while the solid lines represent function (21) for different values of parameter $\Psi$. The asymptotic value of $C_B/(C_B)_N$ in (21) is $1 + e^{\Psi}$, that is, $\Psi$ accounts for the maximum correction allowed as $\mathrm{Ric}_B \to -\infty$. A value $\Psi = \log(2)$ has been chosen using the enveloping curve in Fig. 3.

The resulting estimation of surface fluxes shows that, despite the approximation of constant EF during the

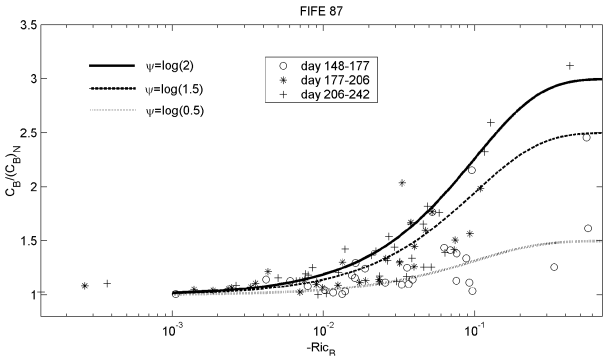


FIG. 3. Ratio of nonneutral to neutral transfer coefficient $C_B$ vs minus bulk Richardson number. The three symbols indicate different periods of the experiment (FIFE 1987). The solid lines are the stability correction function with different values of parameter $\Psi$.

course of the day, the retrieval is accurate even at half-hour scale. Figure 4 is the comparison of the estimated surface fluxes with field measurements. The larger scatter around low flux values in the top row of Fig. 4 is due to the points corresponding to the very first time step of the assimilation interval (i.e., 0900 LT), where the hypothesis of constant EF may be weaker. The root-mean-square difference values are 31.18 W m$^{-2}$ for sensible heat and 56.19 W m$^{-2}$ for latent heat (25.11 and 47.53 W m$^{-2}$, respectively if the 0900 LT points are omitted). The field instrument measurement error itself is about the same magnitude. In the same figure, scatterplots of residual ground heat flux $G$ are reported: note that in this case the flux values are not directly measured but are computed as the residual of the measured values of net radiation and surface turbulent fluxes ($G = R_n - \mathrm{LE} - H$). The influence of the 0900 LT values on the root-mean-square error is even larger in this case.

Finally the results indicate that the system equation as the physical constraint and the radiometric measure-

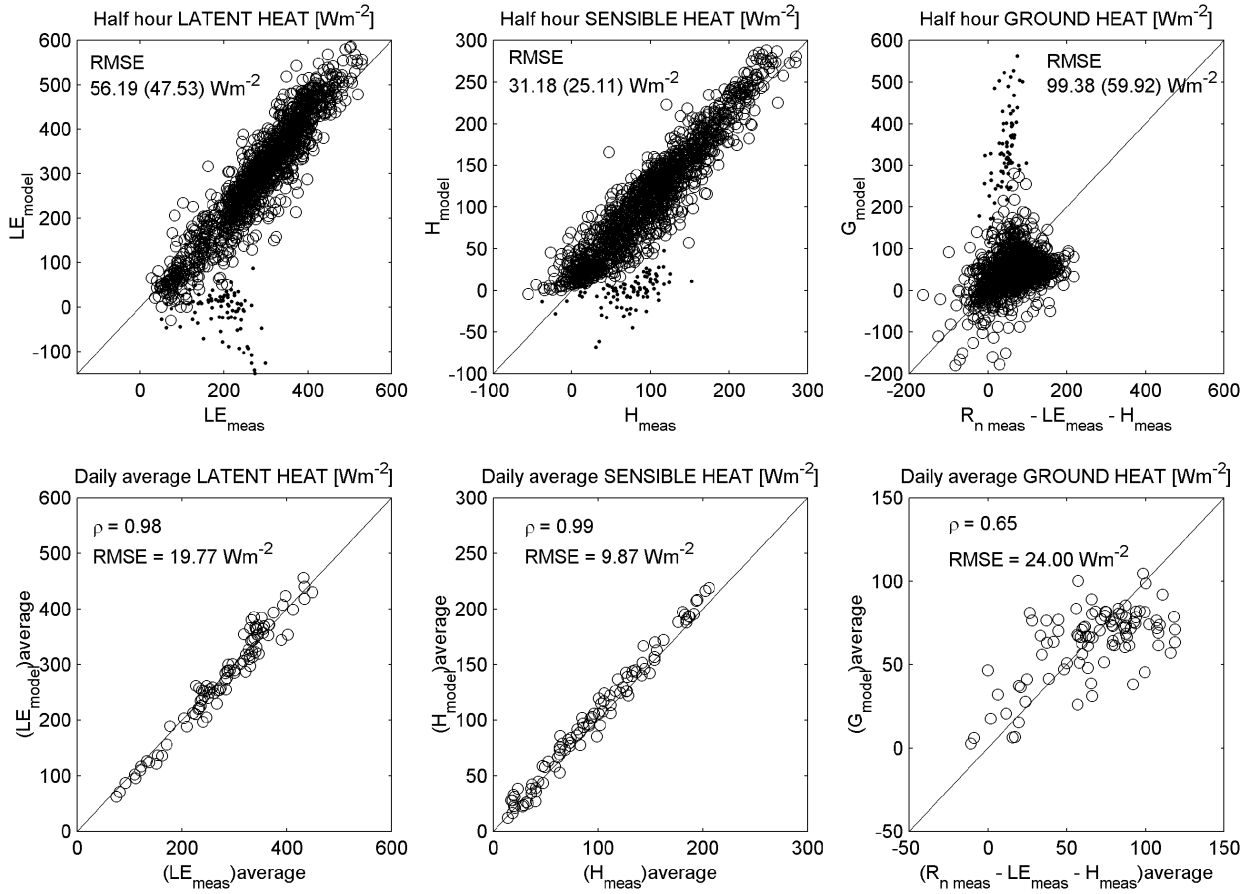


FIG. 4. Measured and estimated (left) latent and (center) sensible heat fluxes and (right) residual ground heat flux $G = R_n - H - \mathrm{LE}$ from measurements and estimation. Estimation corresponds to assimilation with known daily evaporative fraction (FIFE 1987). (top) Scatterplots are half-hourly flux and (bottom) daily averages (0900–1600 LT assimilation window). (top) Larger scatters around low flux values (small dots) are the points corresponding to the initial time of the assimilation interval, which also bring even larger satter in the residual ground heat flux $G$. Root-mean-square differences are reported for each case; (top) values in parentheses are computed without considering the first data point (small dots) of each assimilation interval; correlation is included for daily values only because in the case of the half-hourly data the diurnal cycle dominates the statistic.

ments that are used to characterize the land surface temperature as defined are consistent with one another. Having established this, the more challenging estimation problem when both $R$ and EF are unknown will be tackled next.

### b. Simultaneous estimation of daily EF and bulk transfer coefficient $C_B$

The complete assimilation scheme gives the simultaneous retrieval of the parameters EF and $R$. In this formulation the bulk transfer coefficient is composed of separable free and forced convection components as in $C_B = (C_B)_N f(\mathrm{Ric}_B)$ using (21). Other functional forms of the free convection correction may be used as well. Again the transformation $(C_B)_N = e^R$ is used to ensure that the estimation yields $(C_B)_N > 0$.

In this assimilation daily EF is estimated, that is, an independent value for each day. The variable $R$, which is mostly a function of landscape characteristics (e.g., vegetation phenology) varies on a longer time scale (e.g., monthly). The assimilation windows are arranged in 30-day blocks ($N = 30$) with 15-day overlap. The possibility of simultaneously estimating two parameters ($R$ and EF) from observations of one state variable ($T_s$) is ill posed if the two parameters are allowed to vary at each observation time. By recognizing that EF and $R$ vary on different time scales—daily for EF due to wetting and drying events and monthly for $R$ due to vegetation phenology—the problem may be again well posed. In this way the assimilation system can efficiently distinguish between wet/smooth and dry/rough surfaces since the two estimation variables—in trying to fit land surface temperature fluctuations—vary across different time scales. For each block the update equations for $R$ and EF become

$$R = R' - \frac{1}{K_{C_B}} \sum_N \int_{\tau_0}^{\tau_1} \lambda \frac{\partial \Gamma}{\partial R}\, d\tau$$

$$\mathrm{EF} = \mathrm{EF}' - \frac{1}{K_{\mathrm{EF}}} \int_{\tau_0}^{\tau_1} \lambda \frac{\partial \Gamma}{\partial \mathrm{EF}}\, d\tau. \qquad (22)$$

As mentioned in section 3, the values assigned to the constant parameters ($K_{T_s}$, $K_{C_B}$, $K_{\mathrm{EF}}$) control the rate of convergence of the iterative procedure. These parameters can be related to the error variance of surface temperature if the data assimilation scheme is interpreted in statistical terms. Since the cost function minimum is found iteratively, these parameters also control the rate of numerical convergence and determine the numerical stability of the iterations. In the application here the values ($K_{T_s}$, $K_{C_B}$, $K_{\mathrm{EF}}$) = (5.5 $\mathrm{K}^{-2}$, 0.1, 100) are used. Sensitivity tests were performed to explore the impact of these numerical parameters on the estimation results. There is no significant sensitivity in the retrieved parameters with respect to these constants. The convergence criterion for the iterative scheme is a residual maximum error of 2.0 K in temperature misfit.

Figure 5 shows the comparison between measured and predicted land surface temperature after 500 iterations. The land surface temperature prediction (fit) from the assimilation scheme is reasonably accurate, with a root-mean-square error of 1.11 K for FIFE 1987 and 1.08 K for FIFE 1988.

The retrieved daily evaporative fraction shows a good agreement with the measured values that are in this case withheld for independent verification (Fig. 6). This is true especially over significant drydown periods following rain events. Even though the precipitation events and soil moisture dynamics are totally unknown to the assimilation scheme, the estimated EF shows characteristic response to precipitation wetting and interstorm drydown events.

The assimilation procedure is less robust during an energy-limited or stage-I evaporation regime (when actual evaporation is at or near potential evaporation; see, e.g., the initial period in 1987 experiment). In these conditions, the efficiency of energy dissipation is mainly controlled by atmospheric factors rather than surface properties. The coupling between the evaporative fraction and the surface temperature evolution becomes much weaker and the retrieval of the first one from the second becomes more uncertain. This is evident when the upper limit to EF is included in Fig. 6 as cross symbols. The diagnostic upper-limit $\mathrm{EF}_{\mathrm{pot}}$ can be estimated with (4) by setting $q_s$ in (2) equal to its saturation value, $q_s = q_{\mathrm{sat}}(T_s)$, which results in

$$\mathrm{EF}_{\mathrm{pot}} = \frac{q_{\mathrm{sat}}(T_s) - q_{\mathrm{air}}}{[q_{\mathrm{sat}}(T_s) - q_{\mathrm{air}}] + \dfrac{c_p}{L}(T_s - T_{\mathrm{air}})}, \qquad (23)$$

where $\mathrm{EF}_{\mathrm{pot}}$ as a diagnostic and the EF for stage-I evaporation periods depends only on air temperature, air humidity, and surface temperature. It is possible to pose the estimation scheme in terms of the ratio $\mathrm{EF}/\mathrm{EF}_{\mathrm{pot}}$ when humidity data will be required for the assimilation scheme. The verification of such an approach, however, will require a more extensive set of verification experiments, especially in terms of variability of both climatic and land-type conditions.

As a further test of the robustness of the assimilation system, estimates of EF during overlapping periods are compared in Fig. 6. The root-mean-square error of the differences during the overlaps is small. The values are consistent both in terms of values and day-to-day dynamics across assimilation windows, indicating that the variational scheme has converged to the same minima of the functional $J$.

Figures 7 and 8 show the scatterplots of retrieved half-hour and 0900–1600 LT average fluxes for FIFE 1987 and 1988. In the second block of experiments in FIFE 1987 (corresponding to Julian days 162–192) there are several highly erroneous estimates of fluxes resulting

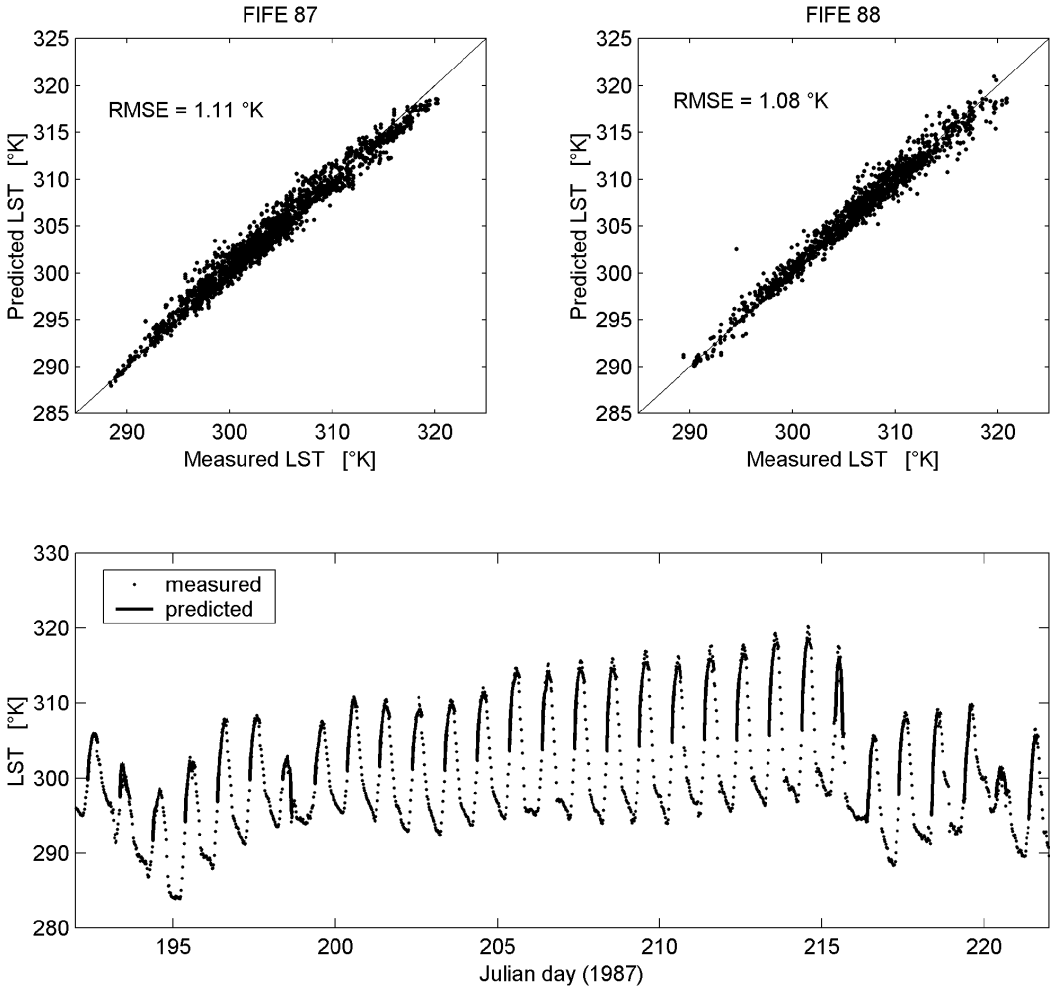


FIG. 5. Comparison between observed and predicted land surface temperature states. (top) Scatterplots of half-hourly measured vs predicted land surface temperature for FIFE 1987 and 1988 experiments, respectively, in the case of simultaneous assimilation of EF and $(C_B)_N$. The root-mean-square errors are reported, while correlation is not shown since in the case of the half-hourly data the diurnal cycle dominates the statistic. (bottom) A sample month-long time series for FIFE 1987.

in wider scatter and higher overall error. During these days the surface is adequately moist and evaporation is at its potential limit.

Over the majority of the days in 1987 and all of the FIFE 1988 days the evaporation estimation is satisfactory, with an overall error on the order of 10%. Figure 9 shows an example of time sequences of measured half-hour latent and sensible heat fluxes and those estimated with the assimilation system.

The retrieved transfer coefficient $(C_B)_N = e^R$ for the periods in FIFE 1987 and 1988 are listed in Table 2. The magnitude of the numbers are within the physically expected range (Stull 1994). In 1987 the trend is for decrease of the coefficient as the summer progresses. In FIFE 1998 the values of $(C_B)_N$ are generally smaller and tend to vary less among the periods. The two summers experienced remarkably different rainfall patterns with notable differences in dominant vegetation phenologies. The summer of 1987 started with major wetting rainstorms and ended with a marked drydown. The summer of 1988 was more similar to the regional summer climatology. Furthermore the patterns of seeding, crop growth, and harvest dates were also reported to have been significantly different. A more in-depth study of these records is required to definitively link the differences between 1987 and 1988 values of $(C_B)_N$ to the surface characteristics.

### *c. Diagnosing the scalar roughness length for heat transfer*

One of the main objectives of the assimilation procedure is the direct estimation of the transfer coefficient $(C_B)_N$. If additional information on the scalar roughness length for momentum transfer (e.g., from wind profile measurements) are available, a diagnosis of the rough-

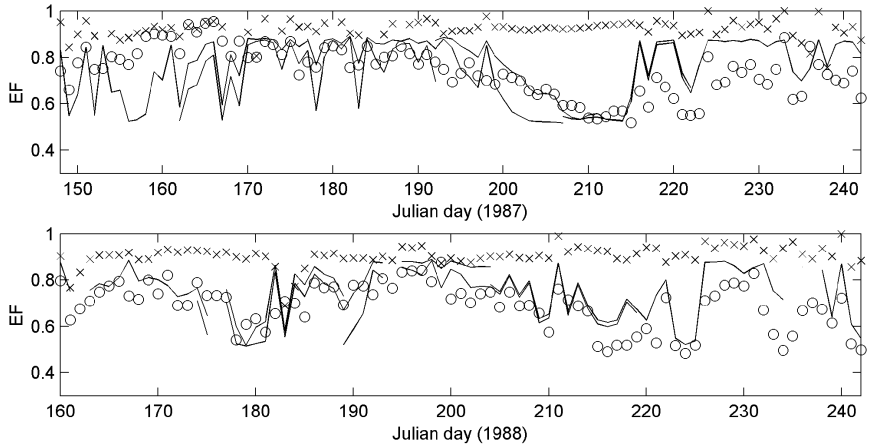


FIG. 6. Evaporative fraction for FIFE 1987 and 1988. [Estimated values from heat fluxes (circles); estimated values from land surface temperature with the variational scheme (lines); $EF_{pot}$ corresponding to potential evaporation (crosses)]. The correlation coefficient between the observed and model-retrieved EF is 0.46 for 1987 and 0.68 for 1988 (including overlapping blocks).

ness length for heat may be attempted as well. Under neutral conditions the bulk transfer coefficient for heat is related to the roughness length scales for heat and momentum transfer ($z_{0H}$ and $z_{0M}$ respectively) as

$$(C_B)_N = \frac{k^2}{\ln\left(\frac{z_{\text{ref}}}{z_{0M}}\right)\ln\left(\frac{z_{\text{ref}}}{z_{0H}}\right)}, \quad (24)$$

where $k \cong 0.4$ is von Karman's constant, $z_{\text{ref}}$ is the common micrometeorological measurement height. In our approach we altogether estimate $(C_B)_N$ as a parameter of the system. For diagnostic purposes the retrieved values of $(C_B)_N$ are inverted for $z_{0H}$ using (24) and published values of $z_{0M}$ at FIFE 1987 (Verma et al. 1992). Analogous estimates of $z_{0M}$ at FIFE for the year 1988 are not available, so the values of $z_{0H}$ are not computed here for that period (see Table 2). The estimation of $z_{0H}$ is always indirect and dependent on the approach and types of measurement. Using radiosonde data Sugita and Brutsaert (1990) report radiometric scalar roughness corresponding to the radiometric surface temperature for the FIFE field site in 1987. Betts and Beljaars (1993) use a different flux formulation and FIFE 1987 aircraft measurements of turbulent flux and radiometric land surface temperature. Sugita and Brutsaert (1990) estimates of $z_{0H}$ varies over several orders of magnitude (order of $10^{-7}$ for spring 1987 average and $10^{-2}$ for fall 1987). Betts and Beljaars (1993) estimate the roughness length for momentum $z_{0M}$ to be 0.19 m and the ratio of this to that for heat to be about 16 (range of 7–35). These values would bring $(C_B)_N$ in the range of (8.6 to 11.5) $\times 10^{-3}$.

## 5. Prospects for application with remote sensing

The new methodology and its tests using FIFE ground-based observations show that sequences of radiometric land surface temperatures contain significant information about land surface evaporation. An interesting extension of the test is to use radiometric surface temperature measurements like those expected from space-borne sensors. This opens the path to large-scale mapping of evaporation fields.

Multispectral remote sensing measurements are needed to estimate land surface temperature. Atmospheric and surface emissivity effects need to be separated from the land temperature in sensor brightness temperature measurements. If multispectral sensors in low-earth orbit are used, then the issue of temporal undersampling becomes an obstacle.

Here an observing system simulation test is introduced to assess the potential sources of error and their magnitudes. Using constellation of low-earth-orbit satellites (current or future) or including geostationary satellites with multispectral sensors will remove this problem altogether. In this study the impact of using only low-earth-orbit platforms is used as an example.

For operational applications using current orbiting platforms, revisits of the same area usually occur no more than twice a day for each satellite. It is likely that for each satellite one of these overpass measurements falls during the period of day when available energy and turbulent fluxes are negligible. When using visible/thermal infrared sensors, presence of clouds may further reduce the sampling. Thus we have to deal with a number of problems that may affect the estimation robustness: (a) the availability of a small number of land surface temperature observations; (b) the possibility that some, or even the majority of, these observations fall outside the nominal assimilation window; (c) the use of different sensors, hence of data with different accuracy and spatial resolutions, to obtain a sufficient number of land surface temperature observations.

The first two problems are more directly linked to the

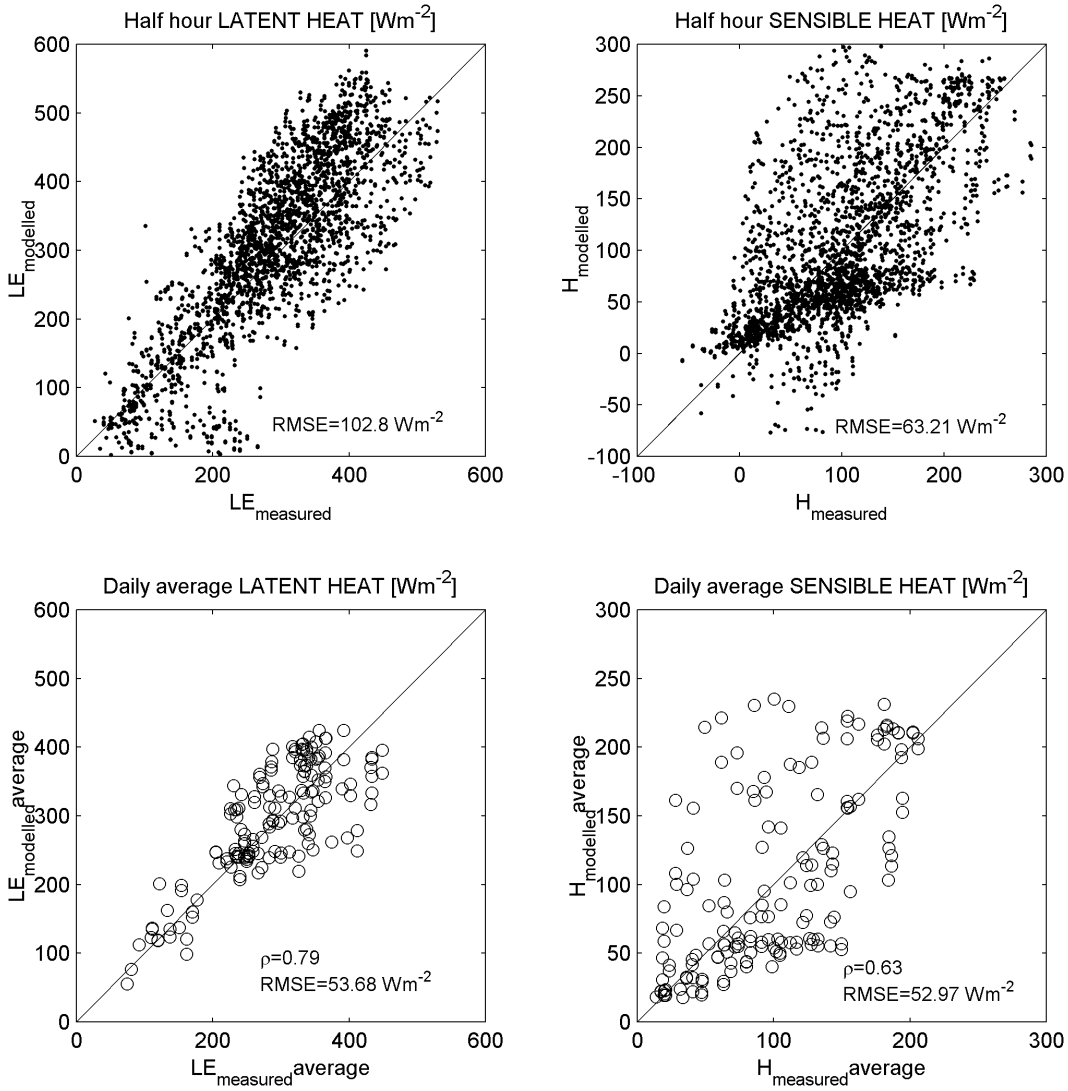


FIG. 7. FIFE 1987 measured vs estimated latent and sensible heat fluxes. Estimation corresponds to assimilation of parameters EF and $(C_B)_N$. (top) Half-hourly flux, (bottom) daily averages (0900–1600 LT assimilation window). Large scatter is observed for the period between Julian days 162 and 192. Root-mean-square error are reported for each case; correlation is included for daily values only because in the case of the half-hourly data the diurnal cycle dominates the statistic.

assimilation methodology presented here. A new set of tests (observing system simulation experiments) of the data assimilation methodology are performed in order to investigate the prospects of application with remote sensing data. The assimilation is performed with only five land surface temperature measurements per day (at 0600, 0730, 1330, 1800, and 1930 LT), that is, a configuration that corresponds to the overpasses of the Advanced Very High Resolution Radiometer [AVHRR instrument on board current National Oceanic and Atmospheric Administration (NOAA) series of satellites] and overpasses of the Special Sensor Microwave Imager [SSM/I on board current series of Defense Meteorological Satellite Program (DMSP) satellites]. Such passes are adequately distributed during the day, so that the retrieval of the diurnal cycle is feasible. A spline interpolation is used to reconstruct the land surface temperature inside the assimilation window at the same time resolution of the micrometeorological measurements. Observations outside the assimilation window, but close to its boundaries, are then also valuable since they properly constrain the interpolation scheme.

The experiment is conducted for the year 1988 and the results show that the estimation of fluxes has an accuracy comparable to the one presented earlier with half-hour data on in situ land surface temperature. In fact the root-mean-square differences between half-hour estimated and measured sensible and latent heat fluxes

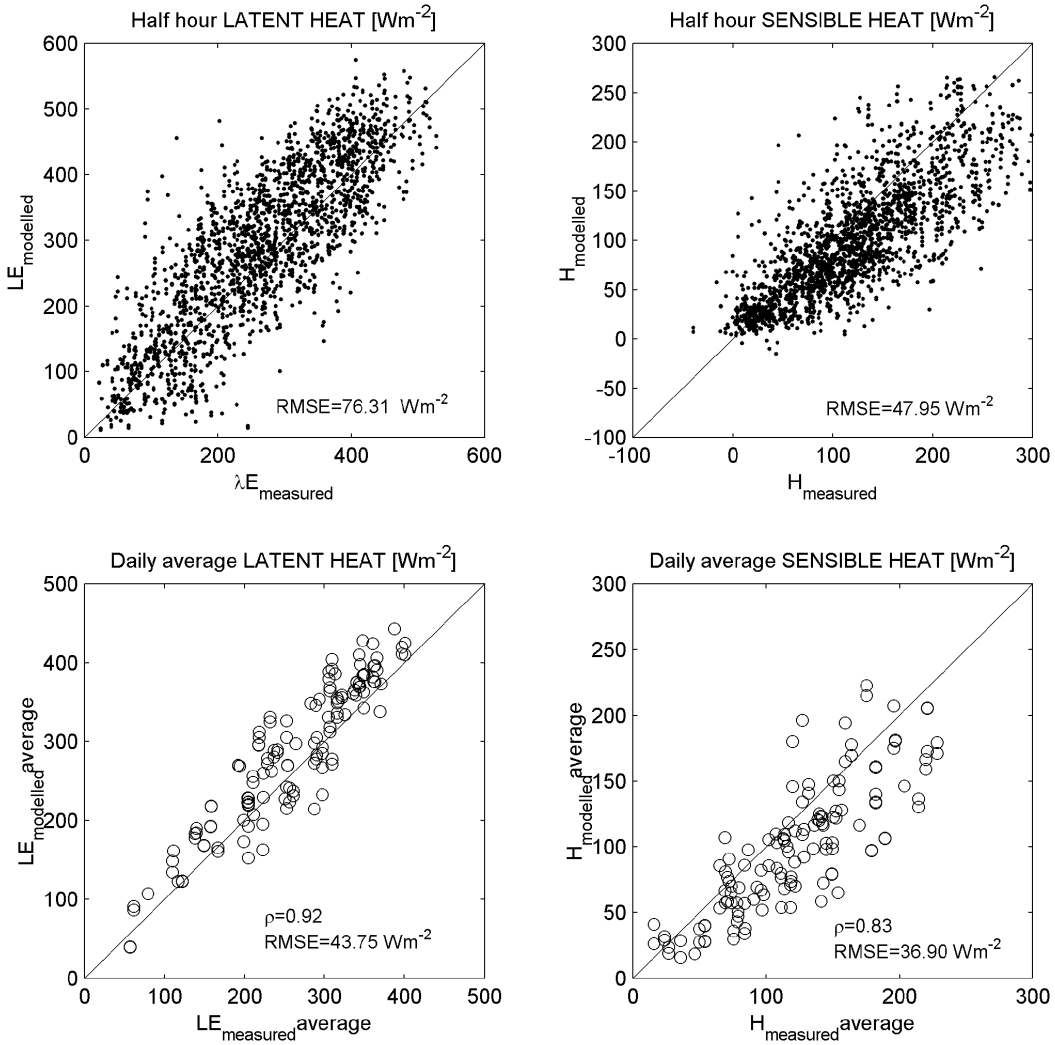


FIG. 8. The same as in Fig. 7 except for FIFE 1988. Note scatter pattern is different.

are in this case 77.89 and 50 W m$^{-2}$, respectively, while using all half-hourly radiometric surface temperature such errors were 76.31 and 47.95 W m$^{-2}$ (see Fig. 8).

## 6. Concluding remarks

A new methodology is introduced to retrieve two important factors required for estimating the components of the land surface energy balance: 1) Moisture-related surface control on evaporation (represented here as the dimensionless evaporative fraction EF), and 2) surface turbulent transfer efficiency (represented here as the dimensionless scalar bulk transfer coefficient $C_B$). Sequences of ground-based radiometric surface temperature measurements are used to infer these two variables in a variational land data assimilation system. The methodology is developed and tested using observations at the FIFE field experiment (summer 1987 and 1988) where surface turbulent flux measurements are available for independent verification.

The methodology is implemented and tested in a stepwise fashion in order to assess the estimation identifiability. In a first test using FIFE 1987 data the daily value of EF is specified and the unknowns are values of $C_B$ over the diurnal cycle. Despite the fact that this surface turbulent characteristic is not known and had to be estimated, the surface energy balance components over the course of the diurnal cycle are captured well. The estimation errors are at the limit of validation data observation uncertainty. The structure of the system equation that serves as the constraint on the estimation is considered to hold well. In this test the retrieved bulk transfer coefficient has a diurnal cycle that is consistent with daily variations in forced convection and measures of boundary layer static stability.

The methodology is then applied to the full problem, that is, simultaneous estimation of EF and $C_B$. Due to the different time scales of variation of the soil moisture dynamics (i.e., EF) and roughness information (i.e., the neutral part $(C_B)_N$ of the bulk transfer coefficient for

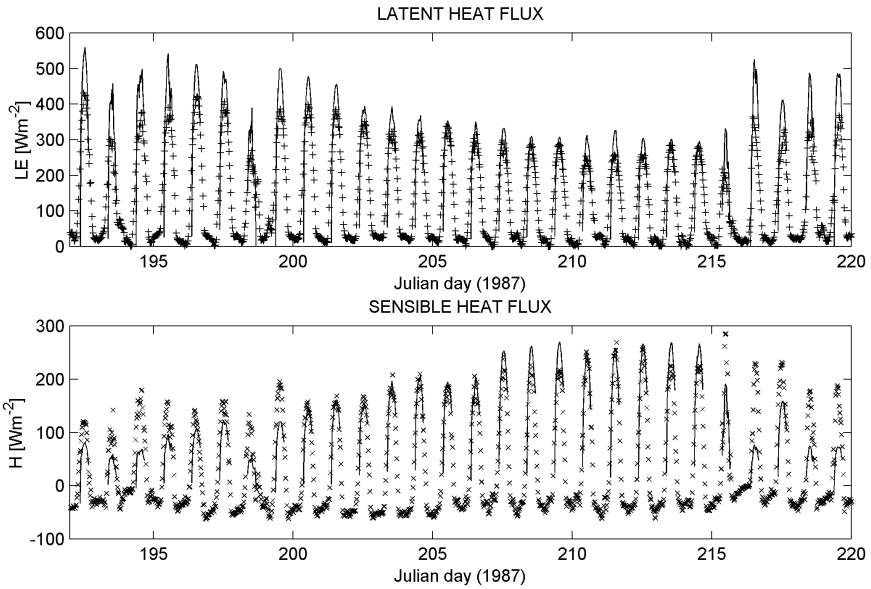


FIG. 9. FIFE 1987 (Julian days 192–220) time series of measured turbulent fluxes (symbols) and estimation values from the assimilation scheme (lines). (top) Latent heat flux and (bottom) sensible heat flux.

heat), the observed land surface temperature can still be efficiently inverted in the estimation of two independent parameters. The estimated daily EF for both FIFE 1987 and 1988 shows dynamics that correspond to intermittent wetting and drydown periods even though precipitation information is completely withheld from the assimilation system. Observed and estimated EF correspond well except for periods when evaporation approaches its potential value, that is, surface moisture is not controlling evaporation and therefore its signature is not evident in radiometric surface temperature sequences. The surface turbulent fluxes at the half-hourly and daily aggregation levels are also estimated with reasonable error values given that neither surface moisture nor turbulent characteristics were known other than that implicit in the radiometric surface temperature sequences.

A main advantage of the way the problem is formulated is that it has limited requirements for ancillary landscape data (e.g., soil texture and vegetation characteristics) and empirical relations. The minimum required data include standard micrometeorological observations of air temperature, wind speed, and net radiation for forcing and radiometric surface temperature for estimation. A major objective of the study is to prepare the path for using satellite remote sensing of radiometric surface temperature. This will enable mapping of surface fluxes and energy balance components. In a final test presented in the paper the FIFE ground-based radiometric surface temperature measurements are undersampled as expected from overpasses of existing orbiting satellite sensors. It is shown that given measurement sequences expected from the overpass times of the current suite of satellites, estimation of surface flux fields is feasible.

*Acknowledgments.* This study has been supported by U.S. and Italian space agencies [National Aeronautics and Space Administration (NASA) and Agenzia Spaziale Italiana (ASI)]. Partial funding from NASA (NAG5-6394) and the Massachusetts Institute of Technology–Consiglio Nazionale delle Ricerche of Italy cooperative agreement for the study of hydrogeologic hazards and climate change are acknowledged.

TABLE 2. Retrieved values of the neutral component of the bulk heat transfer coefficient $(C_B)_N$ for FIFE 1987 and 1988, and roughness length $z_{0H}$ for FIFE 1987.

| FIFE 1987 | | | FIFE 1988 | |
|---|---|---|---|---|
| Julian days | $(C_B)_N$ | $z_{0H}$ [m] | Julian days | $(C_B)_N$ |
| 148–177 | $8.96 \times 10^{-3}$ | $8.69 \times 10^{-2}$ | 160–190 | $1.91 \times 10^{-3}$ |
| 162–192 | $13.4 \times 10^{-3}$ | $2.92 \times 10^{-1}$ | 175–205 | $2.34 \times 10^{-3}$ |
| 177–206 | $7.12 \times 10^{-3}$ | $2.07 \times 10^{-2}$ | 190–220 | $3.76 \times 10^{-3}$ |
| 192–221 | $4.31 \times 10^{-3}$ | $3.40 \times 10^{-4}$ | 205–235 | $3.61 \times 10^{-3}$ |
| 207–242 | $4.60 \times 10^{-3}$ | $5.42 \times 10^{-4}$ | 220–243 | $3.59 \times 10^{-3}$ |

## REFERENCES


Bennett, A. F. 1992: *Inverse Methods in Physical Oceanography*. Cambridge University Press, 346 pp.

Betts, A. K., and C. M. Beljaars, 1993: Estimation of effective roughness length for heat and momentum from FIFE data. *Atmos. Res.*, **30,** 251–261.

——, and J. H. Ball, 1998: FIFE surface climate and site-averaged dataset 1987–89. *J. Atmos. Sci.*, **55,** 1091–1108.

Bhumralkar, C. M., 1975: Numerical experiments on the computation of ground surface temperature in an atmospheric general circulation model. *J. Appl. Meteor.*, **14,** 1246–1258.

Boni, G., D. Entekhabi, and F. Castelli, 2000: Land data assimilation with satellite measurements for the estimation of surface energy balance components and surface control on evaporation. *Water Resour. Res.*, **37,** 1713–1722.

Cahill, A. T., M. B. Parlange, T. J. Jackson, P. E. O'Neill, and T. J. Schmugge, 1999: Evaporation from nonvegetated surfaces: Surface aridity methods and passive microwave remote sensing. *J. Appl. Meteor.*, **38,** 1346–1351.

Carlson, T. N., 1986: Regional-scale estimates of surface moisture availability and thermal inertia using remote thermal measurements. *Remote Sens. Rev.*, **1,** 197–247.

——, J. K. Dodd, S. G. Benjamin, and J. N. Cooper, 1981: Satellite estimation of the surface energy balance, moisture availability and thermal inertia. *J. Appl. Meteor.*, **20,** 67–87.

——, W. J. Capehart, and R. R. Gillies, 1995a: A new look at the simplified method for remote sensing of daily evapotranspiration. *Remote Sens. Environ.*, **54,** 161–167.

——, R. R. Gillies, and T. J. Schmugge, 1995b: An interpretation of methodologies for indirect measurement of soil water content. *Agric. For. Meteor.*, **77,** 191–205.

Castelli, F., D. Entekhabi, and E. Caporali, 1999: Estimation of surface heat flux and an index of soil moisture using adjoint-state surface energy balance. *Water Resour. Res.*, **35,** 3115–3125.

Chen, F., Z. Janjc, and K. Mitchell, 1997: Impact of surface-layer parameterizations in the new land-surface scheme of the NCEP Mesoscale Eta model. *Bound.-Layer Meteor.*, **85,** 391–421.

Crago, R. D., 1996: Conservation and variability of the evaporative fraction during the daytime. *J. Hydrol.*, **180,** 173–194.

——, 1998: Radiometric and equivalent isothermal surface temperatures. *Water Resour. Res.*, **34,** 3017–3023.

——, and W. Brutsaert, 1996: Daytime evaporation and self-preservation of the evaporative fraction and the Bowen ratio. *J. Hydrol.*, **178,** 241–255.

Dickinson, R. E., 1988: The force–restore model for surface temperatures and its generalizations. *J. Climate*, **1,** 1086–1097.

Gillies, R. R., T. N. Carlson, J. Cui, W. P. Kustas, and K. S. Humes, 1997: A verification of the ''triangle'' method for obtaining surface soil water content and energy fluxes from remote measurements of the Normalized Difference Vegetation Index (NDVI) and surface radiant temperature. *Int. J. Remote Sens.*, **18,** 3145–3166.

Idso, S. B., R. D. Jackson, and R. J. Reginato, 1976: Compensating for environmental variability in the thermal inertia approach to remote sensing of soil moisture. *J. Appl. Meteor.*, **15,** 811–817.

Jackson, R. D., 1982: Soil moisture inferences from thermal infrared measurements of vegetation temperatures. *IEEE Trans. Geosci. Remote Sens.*, **20,** 282–286.

Jasinski, M. F., and R. D. Crago, 1999: Estimation of vegetation aerodynamic roughness of natural regions using frontal area density determined from satellite imagery. *Agric. For. Meteor.*, **94,** 65–77.

Jiang, L., and S. Islam, 2001: Estimation of surface evaporation map over southern Great Plains using remote sensing data. *Water Resour. Res.*, **37,** 329–340.

Ma, J., and S. M. Daggupaty, 2000: Using all observed information in a variational approach to measuring $z_{0m}$ and $z_{0t}$. *J. Appl. Meteor.*, **39,** 1391–1401.

Mahfouf, J. F., and J. Noilhan, 1991: Comparative study of various formulations of evaporation from bare soil using in situ data. *J. Appl. Meteor.*, **30,** 1354–1365.

Matsushima, D., and J. Kondo, 1997: A proper method for estimating sensible heat flux above a horizontal-homogeneous vegetation canopy using radiometric surface observations. *J. Appl. Meteor.*, **36,** 1696–1711.

McFarland, M. J., L. Miller, and C. M. U. Neale, 1990: Land surface temperature derived from the SSM/I passive microwave brightness temperatures. *IEEE Trans. Geosci. Remote Sens.*, **28,** 839–845.

Mecikalski, J. R., G. R. Diak, M. C. Anderson, and J. M. Norman, 1999: Estimating fluxes on continental scales using remotely sensed data in an atmospheric–land exchange model. *J. Appl. Meteor.*, **38,** 1352–1369.

Moran, M. S., T. R. Clarke, Y. Inoue, and A. Vidal, 1994: Estimating crop water deficit using the relation between surface-air temperature and spectral vegetation index. *Remote Sens. Environ.*, **49,** 246–263.

Nemani, R. R., and S. W. Running, 1989: Estimation of regional surface resistance to evapotranspiration from NDVI and thermal-IR AVHRR data. *J. Appl. Meteor.*, **28,** 276–284.

Norman, J. M., W. P. Kustas, P. H. Prueger, and G. R. Diak, 2000: Surface flux estimation using radiometric temperature: A dual-temperature-difference method to minimize measurements errors. *Water Resour. Res.*, **36,** 2263–2274.

Pozo Vazquez, D., F. J. Olmo Reyes, and L. Alados Arboledas, 1997: A comparative study of algorithms for estimating land surface temperature from AVHRR data. *Remote Sens. Environ.*, **62,** 215–222.

Price, J. C., 1982: On the use of satellite data to infer surface fluxes at meteorological scales. *J. Appl. Meteor.*, **21,** 1111–1122.

Prigent, C., and W. R. Rossow, 1999: Retrieval of surface and atmospheric parameters over land from SSM/I: Potential and limitations. *Quart. J. Roy. Meteor. Soc.*, **125,** 2379–2400.

Qin, Z., and A. Karnieli, 1999: Progress in remote sensing of land surface temperature and ground emissivity using NOAA–AVHRR data. *Int. J. Remote Sens.*, **20,** 2367–2393.

Raupach, M. R., 1989: Applying Lagrangian fluid mechanics to infer scalar source distributions from concentration profiles in plant canopies. *Agric. For. Meteor.*, **47,** 85–108.

Schaudt, K. J., and R. E. Dickinson, 2000: An approach to deriving roughness length and zero-plane displacement height from satellite data, prototyped with BOREAS data. *Agric. For. Meteor.*, **104,** 143–155.

Sellers, P. J., F. G. Hall, G. Asrar, D. E. Strebel, and R. E. Murphy, 1992: An overview of the First International Land Surface Climatology Project (ISLSCP) Field Experiment (FIFE). *J. Geophys. Res.*, **97,** 18 345–18 371.

Stull, R. B., 1994: *An Introduction to Boundary Layer Meteorology*. Kluwer Academic, 666 pp.

Sugita, M., and W. Brutsaert, 1990: Regional surface fluxes from remotely sensed skin temperature and lower boundary layer measurements. *Water Resour. Res.*, **26,** 2937–2944.

Sun, N. Z., 1994: *Inverse Problems in Groundwater Modeling*. Kluwer Academic, 337 pp.

Van Den Hurk, B. J. J. M., and A. A. M. Holstslag, 1997: On the bulk parametrization of surface fluxes for various conditions and parameter ranges. *Bound.-Layer Meteor.*, **82,** 119–134.

Verma, S., J. Kim, and R. J. Clement, 1992: Momentum, water vapor, and carbon dioxide exchange at a centrally located prairie site during FIFE. *J. Geophys. Res.*, **97,** 18 629–18 639.

Williams, C. N., A. Basist, T. C. Peterson, and N. Grody, 2000: Calibration and verification of land surface temperature anomalies derived from the SSM/I. *Bull. Amer. Meteor. Soc.*, **81,** 2141–2156.

Xu, Q., and C. J. Qiu, 1997: A variational method for computing surface heat fluxes from ARM surface energy and radiation balance systems. *J. Appl. Meteor.*, **36,** 3–11.

Zhou, B., and Q. Xu, 1999: Computing surface fluxes from Mesonet data. *J. Appl. Meteor.*, **38,** 1370–1383.